Kinematics and Physics of Celestial Bodies
Vol. 15, No. 5, pp. 291—297, 1999

Kinematika i Fizika Nebesnykh Tel
Vol. 15, No. 5, pp. 387—397, 1999
UDC 523.9

FORMATION OF SMALL-SCALE MAGNETIC ELEMENTS: SURFACE MECHANISM

A. S. Gadun [1], V. A. Sheminova[1], and S. K. Solanki[2]

[1]*Main Astronomical Observatory, National Academy of Sciences of Ukraine*
Golosiiv, 03680 Kyiv-127

[2]*Max-Planck-Institut für Aeronomie*
2 Max-Planck Str., D-37191 Katlenburg-Lindau

We present the first results of a two-dimensional MHD simulation of the solar magnetogranulation. The medium was assumed to be compressible, gravitationally stratified, radiatively coupled, partially ionized, and turbulent. The simulated magnetogranulation evolved over the course of two hours of hydrodynamic (solar) time. A surface (magnetic plume-like) mechanism which forms thin magnetic elements was found to operate during the process of granule fragmentation. The activity of such a mechanism suggests that the magnetogranulation can concentrate and intensify the global magnetic flux at the boundaries of convective cells and can also form nearly vertical compact magnetic flux tubes by involving the weak horizontal photospheric field, which may be, in general, of local (turbulent) nature.

INTRODUCTION

When small-scale magnetic structures were discovered in 1973 [9,24], the investigators became aware of the fact that the major part of the magnetic flux on the Sun, outside sunspots and pores, is concentrated in these thin elements which are no more than several hundred kilometers in size but have magnetic fields of several hundred millitesla.

These features have been the object of much observational and theoretical research (see the reviews by Solanki [22,23], Schüssler [20,21], and Muller [17]). Of special interest is a multidimensional simulation of the interaction between the thermal granulation-scale convection and the magnetic field; this simulation can be done by solving a system of equations of radiative magnetohydrodynamics for an inhomogeneous, compressible, and gravitationally stratified medium. With such time-dependent models the mechanisms of formation of compact magnetic elements can be studied in detail, and the adequacy of the simulation can be tested as well by comparing the calculated and observed Stokes profile parameters of spectral lines.

The initial magnetic field intensity and configuration are important parameters in such calculations. In most studies (e.g., [1,2,13]) the initial field was assumed to be of global nature, and it was therefore homogeneous, vertically oriented, and it filled the entire calculation region. The function of the granulation in this case is to concentrate the magnetic field near the boundaries of convective cells and intensify the field. The simulation in [1,2,13] lasted only from five to nine minutes of hydrodynamic time, and the authors could follow the effect of kinematic and superadibatic mechanisms on the formation of magnetic structures only over the lifetime of those convective flows ("cells") which existed from the outset. The effect of granule fragmentation (diffusion) on the evolution of magnetic structures could not be investigated.

A different initial field was taken by Brandt and Gadun [3]. It also was homogeneous and vertically oriented, but it had the only horizontal scale (70 km), and its initial intensity was 8.5 mT. The time of magnetogranulation simulation was quite long (48 min). However, the granulation convection was assumed to be quasi-stationary rather than nonstationary (two convective flows of the same scale existed in the

dimensional simulation region — the symmetrical initial conditions permitted them to coexist for an indefinitely long time). It was found, nevertheless, that a magnetic configuration with an intensity of about 100 mT may form with such a weak local priming field and a strong convective instability. The topological pumping and the density gradient effect [4] ensure the initial intensification of the magnetic field in deeper layers; the kinematic mechanism concentrates the field lines in the vicinity of downflows. The superadiabatic (thermal) effect is the dominant factor in the intensification of the magnetic field; it grows when the magnetic field energy is close to the equipartition level or exceeds it. In this case the magnetic field suppresses the convective flows, and the magnetic configuration situated in the region of downflows suddenly begins to descend.

So, we may state that all published attempts of the direct numerical simulation of magnetoconvection ignore a fundamental feature of the solar thermal convection — its nonstationarity. There are also some problems in the formulation of initial conditions for the magnetic field.

In this study we present some results of further development of the two-dimensional numerical simulation of magnetogranulation. Nonstationary magnetogranulation was simulated over the course of two hours of hydrodynamic time with the use of a new concept of initial magnetic field. We show that the fragmentation of granules in the presence of horizontal photospheric fields results in the formation of new small-scale magnetic structures. This mechanism is given the name surface mechanism. We think it important for an understanding of magnetogranulation in various objects to establish the role of this mechanism in the formation of flux tubes, but here we only describe it, and a detailed analysis of the simulation results will be published elsewhere.

Small-scale magnetic elements are usually called flux tubes [22,23]. Of course, they are not tubes in the two-dimensional plane representation, but we arbitrarily reserve this traditional name for them.

TWO-DIMENSIONAL RADIATIVE MAGNETOHYDRODYNAMICS

The complete set of equations of radiative MHD for the conditions of compressible gravitationally stratified turbulent medium had the following form:

$$\frac{\partial \rho}{\partial t} + \nabla \rho \mathbf{V} = 0 ,$$

$$\frac{\partial \rho \mathbf{V}}{\partial t} = -\nabla \left[\rho \mathbf{V}\mathbf{V} + \left(P + \frac{B^2}{8\pi} \right) \mathbf{I} - \frac{\mathbf{B}\mathbf{B}}{4\pi} + \mathbf{R} \right] - \rho \mathbf{g} ,$$

$$\frac{\partial \rho U}{\partial t} = -\nabla \left\{ (\rho U + P + \mathbf{R})\mathbf{V} - \frac{\mathbf{B}}{4\pi} (\mathbf{V}\mathbf{B}) + \frac{D_m}{4\pi} [[\nabla, \mathbf{B}], \mathbf{B}] \right\} + \rho q_D - Q_R - \rho g v_z ,$$

$$\frac{\partial \mathbf{A}}{\partial t} = [\mathbf{V}, \mathbf{B}] - D_m [\nabla, \mathbf{B}], \qquad \mathbf{B} = [\nabla, \mathbf{A}].$$

Here A is the vector potential, I is a unit tensor, R is the Reynolds turbulence stress tensor, g(g) is the free fall acceleration, $U = E + B^2/8\pi/\rho$ is the total specific energy ($E = v^2/2 + e$), e is the internal energy, q_D is the kinetic energy dissipation of the averaged motion at the subgrid level, D_m is the magnetic diffusion coefficient, Q_R is the divergence of the radiation flux vector (radiation heating/cooling); the spatial rectangular coordinates x and z describe the simulation region in the horizontal and vertical directions. We also assume the magnetic induction B to be equal to the magnetic field intensity H, the magnetic permeability being equal to 1.

We used the ideal gas equation in our calculations; the radiation pressure and possible changes in the electron density due to hydrogen ionization and double ionization of 15 elements were taken into account. The contribution of H^- and H_2, H_2^+ molecules to the ionization equilibrium was taken into account at $T \leq 6000$ K.

The set of equations and the solution of the transfer equation used to determine Q_R are described in detail in [3,5,6]. The radiation effects were treated in our simulation in the "grey" approximation.

Free upper and lower boundary conditions were taken for velocities and thermodynamic quantities, i.e., the free inflow and outflow of matter were permitted: the velocity components were determined from the condition $\partial \mathbf{V}/\partial z = 0$, and the mean internal energy and mean density were taken from the initial homogeneous model [5,6]. Their fluctuation profiles at the upper (lower) boundary were the same as in the layer situated below (above). The density at the lower boundary was scaled to provide a constant sum of the gas, radiation, and magnetic pressures at the horizontal level. The upper and lower boundary conditions for the magnetic field were set, assuming that it was of global nature: $B_x = 0$, $\partial B_z/\partial z = 0$.

Periodic side conditions were postulated.

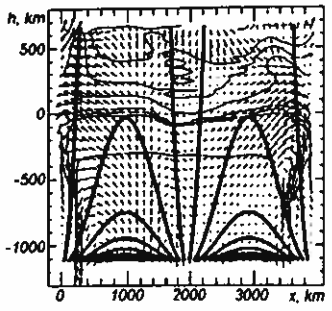

Fig. 1. Initial model and initial magnetic field configuration in the MHD simulation. Thin lines) isotherms for temperatures (from the top down): 4000, 5000, 6000, 7000, 8000, 9000, 10000, and 12000 K. Thick lines) magnetic field lines.

below (above). The density at the lower boundary was scaled to provide a constant sum of the gas, radiation, and magnetic pressures at the horizontal level. The upper and lower boundary conditions for the magnetic field were set, assuming that it was of global nature: $B_x = 0$, $\partial B_z/\partial z = 0$.

Periodic side conditions were postulated.

The size of simulation region was 3920 × 1820 km, the spatial step was 35 km, the atmospheric layers extended over about 700 km. The internal structure of thin magnetic configurations cannot be studied in detail with such a spatial step, but it is sufficiently large for the evolution of these configurations to be followed and the calculation costs to decrease.

We calculated two model sequences with a magnetic field and without field, with the same initial conditions. The initial model was taken from the time series of HD models [10], but the simulation region was diminished.

Figure 1 shows the initial magnetic field configuration and the initial model. This is a bipolar configuration with a field intensity decreasing with height. The mean intensity B was 5.4 mT throughout the calculation region.

After several similar calculation runs with different initial conditions for the magnetic field (including a homogeneous vertically directed field) we concluded that the configuration shown in Fig. 1 is the most natural one (uniformly distributed). It also provides the optimal conditions for the numerical stability of the solution at the initial moment of simulation, since the velocity field and the field of thermodynamic quantities, on the one hand, and the magnetic field characteristics, on the other hand, turn out not to be self-consistent in the initial model.

RESULTS

Figure 2 displays the average value of B in the simulation region as a function of magnetohydrodynamic (real solar) time. The simulation may be arbitrarily divided into three stages — the initial period (to 20 min), which is mainly controlled by the initial conditions adopted for the magnetic field, the transition period, when a mutual rearrangement of the thermal convection and the magnetic field occurs, and finally, the period of self-consistent solutions.

Figure 3 demonstrates the evolution of the magnetic field and the brightness field (visible granulation pattern at a wavelength of 500 nm). The intergranular lanes in Fig. 3*a* are shown by dark hatching and granules are shown by light hatching. The granules and intergranular lanes were distinguished for every individual model with respect to the mean intensity level at λ 500 nm. The areas with intensities above this level were recognized as granules and below this level as intergranular lanes.

The magnetic field for the continuum formation level ($\log\tau_R = 0$, τ_R being the Rosseland optical depth) is shown in Fig. 3*b* with the field polarities hatched differently. In the course of the initial 20 min the concentration and intensification of the magnetic field occur in the vicinity of downflows (x = 3600—3800 km). Then a partial reconnection of field lines takes place (the reason is, in part, that the initial field was taken as bipolar), and local magnetic field concentrations dissipate. Over the period from the 20th to 35th minute there are no marked structures in the magnetic field. A clear-cut structuring in the field concentration is observed afterwards: the field becomes stronger in intergranular lanes. The onset of concentration (formation of new thin magnetic elements) coincides in time and space with the moment when granules break up, and the field separates in

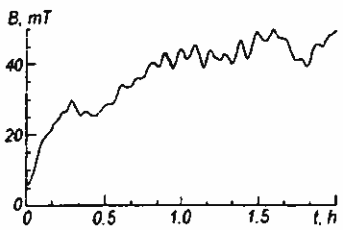

Fig. 2. Evolution of the mean magnetic field intensity in the simulation region.

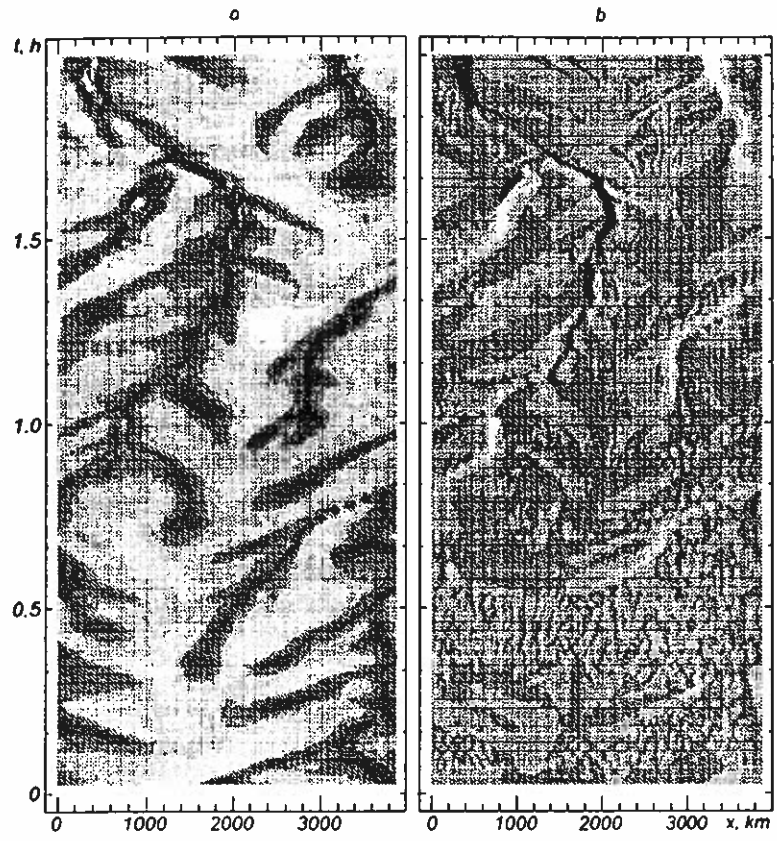

Fig. 3. Spatial and temporal evolution of the emerging monochromatic intensity at λ 500 nm (*a*) and the magnetic field intensity (*b*) in the 2-D MHD simulation. The relative intensity ranges from 0.017 to 1.78 (on a linear scale). The field intensity B ranges from −286.7 to +254.0 mT. Dark hatching) negative polarity field, light hatching) positive polarity field. The field intensity was determined for the continuum formation level, $\log\tau_R = 0$.

polarity at that time as well. The intergranular lanes become brighter when the intensity of magnetic features exceeds 100 mT.

The fragmentation of convective flows is due to the action of surface layers, which serve as a thermal boundary [19]. For example, the Rosseland absorption coefficient decreases by the order of 1000 and the heat capacity by the order of 10 in hot upflows near the visible surface in a height interval as small as 100 km [11]. As a result, the hot thermal flows are intensely cooled (due mainly to radiation losses) and become unstable. As shown in [6,12,18], the mechanism through which the flows lose their stability is determined by their horizontal scale. The flows related to the granules up to $l_g \approx$ 1000—1400 km in size dissipate in the main, while larger flows break up. It was found in [11] from 2-D HD models that of crucial importance for small-scale flows ($l_g \leq$ 600 km) is the thermal decay due to radiation losses predominantly in the horizontal direction. Such flows cool rapidly and dissipate.

Large-scale convective upflows with $l_g \geq$ 1000 km are highly adiabatic, and the major cause of their instability is the excess pressure which develops inside them. This pressure excess is a fundamental property of the thermal convection in stratified media (this was found even with the simplest polytropic models [8]). Its relative magnitude is especially large near the surface (the thermal boundary), and this gives rise to the buoyancy inversion. It is the locality where the adiabatically moving matter penetrates into the photosphere and is slowed down through the radiation cooling. In addition, large horizontal dimensions of convection cells favor the formation of a highly dense passive cloud of matter which hangs over the central parts of convection cells. The excessive pressure forces weaken the central convective flow and tend to redistribute the convective energy flux in the horizontal direction from central regions to periphery. Thereafter the weakened central fragment of the large-scale thermal flow cannot provide the balance of forces to support stability near the surface, and a stream of matter directed from the surface downwards is formed from the dense cloud; the fragmentation thus comes to an end [11].

It was shown in [11] that the flows of intermediate horizontal dimensions (l_g = 600—1000 km) experience the effect of both mechanisms to the least extent. These theoretical results found an observational support [7,14].

The fragmentation of the thermal convective flows in the presence of magnetic fields maintains the formation of new small-scale magnetic elements. It this case the streams of cool matter newly formed near the surface entrap horizontal magnetic field lines, carry them downwards, changing the horizontal orientation of the field to the vertical one, and intensify the field by extending the field lines. The photospheric horizontal magnetic field is quite week, and it meets the freezing-in condition. The field lines are not completely reconnected in this case, since the velocity field is not completely symmetrical in the convective cell which

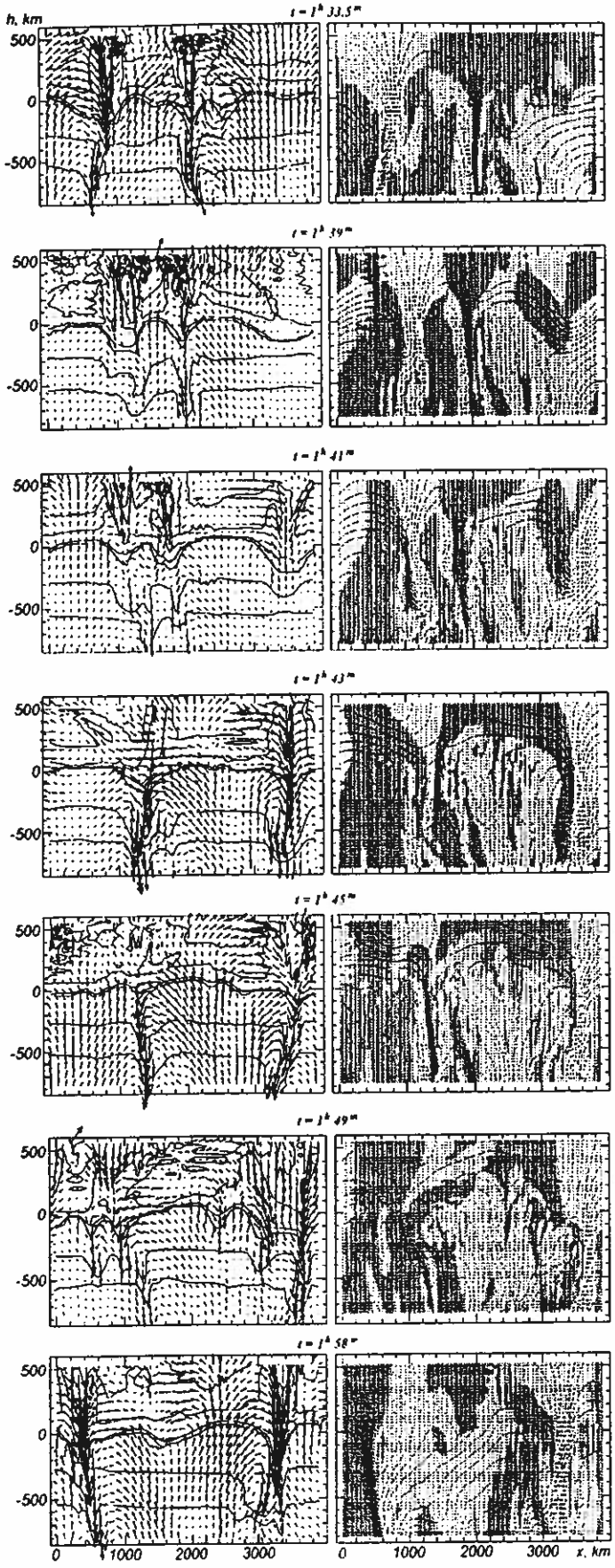

undergoes fragmentation and the cell itself displays clear-cut polarities, with the field intensity growing with depth.

Figure 4 illustrates the mechanism described above. The time in this figure corresponds to the time scale in Fig. 3, so that the magnetogranulation evolution can be followed in parallel in both figures. The first fragment represents the situation obtained in the calculation region after $1^h33.5^m$ of modeling. Two flux tubes of opposite polarities are concentrated in intergranular lanes. In the right part of the region ($x > 2200$ km) a well-developed convective flow (a granule) is located and suppression of the central fragment has already begun in the lower part of this flow.

A characteristic feature at the moment 1^h39^m is the onset of fragmentation in the large-scale flow: the surface level between $x \approx$ ≈ 3300 km and $x \approx 3700$ km is sagged, and the horizontal magnetic field lines begin to sag as well.

The fragmentation progresses further from 1^h41^m to 1^h43^m: an active downflow develops due to the convective instability. The field lines are entrained by it. No complete reconnection of the entrained field lines is observed, as the convective cell itself has clear-cut polarities in the area where the downflow is passing and the field intensity grows with depth inside the sell in accordance with the equipartition condition. The field of one polarity only is intensified (the positive polarity in this case), and the field of the other polarity weakens (1^h45^m).

Finally, in the time interval from 1^h45^m to 1^h58^m well-developed flux tubes are observed: one tube ($x \approx 3200$—3400 km) was formed by the above mechanism, and the second tube ($x \approx 400$—600 km) appeared due to the kinematic effect. However, the superadiabatic (or thermal) mechanism plays the major role in the field intensification in both cases; it is associated with the superconvective instability

Fig. 4. Velocity field and temperature (on the left), magnetic field lines and field polarity (on the right) for selected simulation moments. Horizontal lines on the left) 4000, 5000, 6000, 7000, 12000, and 13000 K isotherms (from the top down). Dark hatching) negative polarity field, light hatching) positive polarity field.

of downflows in the presence of strong magnetic fields.

The figures demonstrate not only the formation of flux tubes but their dissipation as well — the tube found between $x = 600$ km and $x = 800$ km at $1^h33.5^m$ dissipated completely by the moment 1^h43^m, and another compact magnetic configuration, between 2000 and 2200 km, weakens significantly and disappears as a bright feature in an intergranular region.

Compact fields dissipate in our models due to two mechanisms: the internal instability of such intensive small-scale features and their weakening caused by reconnection of field lines. The internal instability of flux tubes was studied in detail in [13]: it develops in intensive magnetic structures of a larger scale as a result of potent convective instability — this instability gives rise to an intense evaporation of the matter in the subphotospheric layers inside the tube. Under the conditions governing in a gravitationally stratified medium this inevitably leads to the expansion of matter along field lines from deeper layers and the "reversion" of the superadiabatic effect — downflows are replaced by upflows inside the tube. The fields become less compact, and the tube breaks down.

The other mechanism is clearly recognized in our simulation. It, in essence, is this: the tube and the adjacent regions of convective cells may be of different polarities, and the kinematic effect, which steadily squeezes the field out of cells, weakens the tube in the intergranular region owing to the reconnection of field lines.

An interesting effect is produced by the common operation of the kinematic mechanism and the thermal one in the concentration and intensification of the magnetic field — newly formed compact structures with strong magnetic fields and areas with relatively weak fields of opposite polarity may be next to one another. This effect can be seen in Figs 3 and 4, and it is confirmed by observations of magnetic regions with high spatial resolution [15,16].

Thus, the role of granulation in the formation of small-scale magnetic structures should be revised. While it was originally assumed that it only concentrates the global large-scale magnetic field in bundles at cell boundaries, our calculations suggest that it is capable of forming thin magnetic tubes from the weak photospheric horizontal field. The existence of this field is confirmed by observations. In his controversial paper [21] Schüssler gives the observed distribution of the magnetic field inclination as a function of field intensity. This distribution suggests that weak fields are predominantly horizontal in the photospheric layers, and so the mechanism described above is quite realistic.

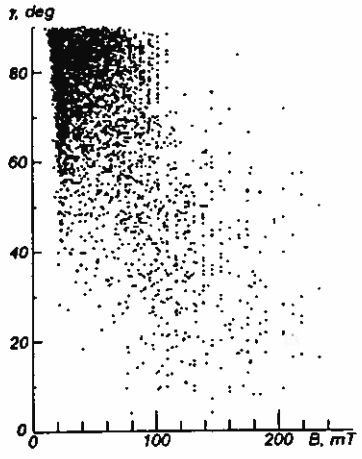

Fig. 5. Theoretical dependence of the magnetic field inclination γ on the field intensity B.

We obtained a similar distribution (Fig. 5) from our models by simulating spectral observations during the last 25 min of the MHD modeling. First we calculated the Stokes profiles for the IR Fe I line λ 1564.8 nm (it is often used in observation programs). Then we applied the well-known Stokes diagnostics techniques to the theoretical spectral "scans" in order to determine the inclination of the magnetic field to the vertical, γ, and the field intensity B. The inclination angle was found from the relation $\tan\gamma = \sqrt{Q}/V$ (this is an approximate relation, and it is evident from the known expressions for the amplitudes of the σ-components of the V, Q, and U Stokes profiles), and the field intensity was estimated from the distance between the peaks in the red and blue wings of the V profile. In view of a lower spatial resolution of the observations, the agreement between the observed and theoretical distributions is quite good. This is one more argument for revising the concept of the formation of small-scale magnetic elements.

CONCLUSION

A direct numerical simulation of the magnetoconvection on the granulation scales suggests that the role of granulation in the formation of small-scale magnetic structures should be revised. The granulation can concentrate the magnetic field in bundles on the boundaries of convective cells and enhance the field intensity in them, but it can also form small-scale flux tubes from weak horizontal fields, which may be, in principle, of local nature.

This study was partially financed by the Swiss National Science Foundation (Grant No. 7UKPJ 48440).

References

1. I. N. Atroshchenko and V. A. Sheminova, "Numerical simulation of the interaction between solar granules and small-scale magnetic fields," Kinematika i Fizika Nebes. Tel [Kinematics and Physics of Celestial Bodies], vol. 12, no. 4, pp. 32—45, 1996.

2. I. N. Atroshchenko and V. A. Sheminova, "Simulation of spectral effects with the use of two-dimensional magnetohydrodynamic models of the solar photosphere," ibid., no. 5, pp. 32—47, 1996.

3. P. N. Brandt and A. S. Gadun, "Changes in the Fe II line parameters depending on magnetic flux (solar disk center)," ibid., vol. 11, no. 4, pp. 44—59, 1995.

4. S. I Vainshtein, Ya. B. Zel'dovich, and A. A. Ruzmaikin, Turbulent Dynamo in Astrophysics [in Russian], Nauka, Moscow, 1980.

5. A. S. Gadun, "Multidimensional hydrodynamics models of the solar atmosphere: effects of radiative transfer in a multidimensional perturbed medium," Kinematika i Fizika Nebes. Tel [Kinematics and Physics of Celestial Bodies], vol. 11, no. 3, pp. 54—72, 1995.

6. A. S. Gadun and Yu. Yu. Vorob'ev, "Characteristics of artificial granules in a two-dimensional numerical hydrodynamic simulation of solar granulation," Astron. Zhurn., vol. 73, no. 4, pp. 623—632, 1996.

7. V. N. Karpinskii and N. M. Pravdyuk, "Is the solar granulation a fractal structure?," Kinematika i Fizika Nebes. Tel [Kinematics and Physics of Celestial Bodies], vol. 14, no. 2, pp. 119—129, 1998.

8. R. J. Bray, R. F. Loughhead, and C. J. Durrant, The Solar Granulation, pp. 95—246, Univ. Press., Cambridge, 1984.

9. R. B. Dunn and J. B. Zirker, "The solar filigree," Solar Phys., vol. 33, no. 2, pp. 281—304, 1973.

10. A. S. Gadun, S. K. Solanki, and A. Johannesson, "Granulation near the solar limb: observations and 2-D modeling," in: Motions in the Solar Atmosphere, pp. 201—204, Kluwer, Dordrecht, 1999.

11. A. S. Gadun, S. K. Solanki, S. R. O. Ploner, et al., Scale-Dependent Properties of 2-D Artificial Solar Granulation, Kyiv (MAO NAS Ukraine Preprint No. MAO-98-4E), 1998.

12. A. S. Gadun and Yu. Yu. Vorob'yov, "Artificial granules in 2-D solar models," Solar Phys., vol. 159, no. 1, pp. 45—51, 1995.

13. U. Grossmann-Doerth, M. Schüssler, and O. Steiner, "Convective intensification of solar surface magnetic fields: results of numerical experiments," Astron. and Astrophys., vol. 337, no. 3, pp. 928—939, 1998.

14. I. Kawaguchi, "Morphological study of the solar granulation. II," Solar Phys., vol. 65, no. 2, pp. 207—220, 1980.

15. S. Koutchmy, "High spatial resolution observations of magnetic flux elements," in: Solar Polarimetry, pp. 237—250, NSO, Sunspot, 1991.

16. S. Koutchmy, J. B. Zirker, T. Darvann, et al., "High spatial resolution V-Stokes polarimetry to measure the Zeeman effect in flux tubes and prominence filament threads," ibid., pp. 263—271.

17. R. Muller, "Properties of small magnetic elements," in: Solar Surface Magnetism, pp. 55—72, Kluwer, Dordrecht, 1994.

18. S. R. O. Ploner, S. K. Solanki, A. S. Gadun, and A. Hanslmeier, "Temporal evolution of artificial solar granules," Space Sci. Rev., vol. 85, pp. 261—268, 1998.

19. M. P. Rast, Å. Nordlund, R. F. Stein, and J. Toomre, "Ionization effects in three-dimensional solar granulation simulations," Astrophys. J., vol. 408, no. 1, pp. L53—L56, 1993.

20. M. Schüssler, "Theoretical aspects of small-scale photospheric magnetic fields," in: Solar Photosphere: Structure, Convection and Magnetic Fields, pp. 161—179, Kluwer, Dordrecht, 1990.

21. M. Schüssler, "The solar photosphere: open questions," in: A Crossroads for European Solar and Heliospheric Physics: Recent Achievements and Future Mission Possibilities, ESA SP-417, 1998.

22. S. K. Solanki, "Empirical models of photospheric flux tubes," in: Solar Photosphere: Structure, Convection and Magnetic Fields, pp. 103—120, Kluwer, Dordrecht, 1990.

23. S. K. Solanki, "Small-scale solar magnetic fields: an overview," Space Sci. Rev., vol. 63, pp. 1—188, 1993.

24. J. O. Stenflo, "Magnetic-field structure of the photospheric network," Solar Phys., vol. 32, no. 1, pp. 41—63, 1973.

24 May 1999